AIP | The Journal of Chemical Physics

Electronic structure and reactivity in water splitting of the iron oxide dimers and their hexacarbonyls: A density functional study

Ellie L. Uzunova and Hans Mikosch

Citation: The Journal of Chemical Physics **140**, 024303 (2014); doi: 10.1063/1.4858462
View online: http://dx.doi.org/10.1063/1.4858462
View Table of Contents: http://scitation.aip.org/content/aip/journal/jcp/140/2?ver=pdfcov
Published by the AIP Publishing

Electronic structure and reactivity in water splitting of the iron oxide dimers and their hexacarbonyls: A density functional study

Ellie L. Uzunova[1,a)] and Hans Mikosch[2]
[1]*Institute of General and Inorganic Chemistry, Bulgarian Academy of Sciences, Sofia 1113, Bulgaria*
[2]*Institute for Chemical Technologies and Analytics, Vienna University of Technology, Getreidemarkt 9/E164-EC, 1060 Vienna, Austria*

(Received 26 August 2013; accepted 13 December 2013; published online 8 January 2014)

The iron oxide dimers $(FeO)_2$ and their peroxide isomers are studied with the B3LYP density functional as bare clusters and as hexacarbonyls. Among the bare clusters the planar four-member ring structures are more stable than the non-planar ones and the rhombic dioxide Fe_2O_2 with antiferromagnetically ordered electrons on iron centers is the global minimum. Water adsorption on the bare diiron dioxide is exothermic, but dissociation does not occur. Carbonylation favors a non-planar Fe_2O_2 ring for both the dioxides and the peroxides and high electron density at the Fe centers is induced, evidenced by the natural charge distribution, the high proton affinity, and the values of global electronegativity and hardness. The iron dioxide hexacarbonyl $Fe_2O_2(CO)_6$ is diamagnetic in the state of the global minimum. It is separated from the next low-lying triplet state by a small energy gap of 0.22 eV. Time-dependent density functional theory methods were applied to examine electron excitations from the ground state to the low-lying triplet states in the hexacarbonyls and their adsorption complexes with water. Singlet-to-triplet state excitations occur via ligand-to-metal charge transfer in the hexacarbonyls; in the adsorption complexes excitations from the oxygen lone pairs to the adsorption center also occur and they appear in the IR-visible region. The lowest energy singlet and triplet state reaction paths for water splitting were followed. On the singlet potential energy surface (PES), water splitting is spontaneous, while for the triplet PES an activation barrier of 14.1 kJ mol^{-1} was determined. © *2014 AIP Publishing LLC*. [http://dx.doi.org/10.1063/1.4858462]

I. INTRODUCTION

The iron oxide clusters are among the most extensively studied oxide species of the 3d elements.[1–15] Theoretical and experimental studies have been devoted to both mononuclear oxide clusters[9–14] and to larger ones Fe_nO_m (n = 2–12, m = 1–12).[8,11,15] The reversible oxidation-reduction properties of iron cations in oxides presume their role in catalytic redox reactions and iron oxides are component of industrial catalysts.[16] In the search for improved catalytic and photocatalytic materials active in the reaction of water splitting, iron oxides have been examined in the form of nanocrystals and thin hematite layers.[17,18] On the hematite (α-Fe_2O_3) surface water adsorbs dissociatively, and density functional theory (DFT) studies shed light on the reaction path and the energy barriers at different surface terminations.[19] The molecular approaches towards efficient artificial photosynthetic systems, however, remain a challenge.[20] The binuclear coordination compounds of oxygen-bridged transition metal cations which possess more than one stable oxidation state are promising, because they present two active sites with electron-donor (acceptor) properties. Structures of the cyclic dimers of transition metal monoxides are known to be stable as bare clusters, which can react further with oxygen, or form larger oxide nanoclusters.[8,13,21] The metal-oxide dimers are the simplest models, to which accurate theoretical methods can be applied (coupled cluster method, Brueckner doubles) and compared with experimental data. Multinuclear oxide clusters of the 3d elements (Sc-Cu) were studied experimentally both in gas-phase and as matrix-isolated species.[21] The iron oxide cyclic dimer was detected in the IR spectra of matrix-isolated Fe_nO_m species; gas-phase frequencies were deduced from photoelectron studies of monoanions.[3–6,22] DFT studies with basis sets of moderate size denoted a triplet state of the rhombic $(FeO)_2$ cluster as the global minimum.[22] A later study suggested the $^7B_{2u}$ state as the one of lowest energy,[23] but recent studies of spin coupling at the Fe centers proved antiferromagnetic ordering in the ground state dimer.[13] Among the monocations $Fe_nO_m^+$ with ($n < 6$, $n \leq m$), those with Fe/O ratio 1:1, $(FeO)_n^+$, were found to be more stable than the clusters with either excess of oxygen or excess of iron.[15] Experimental and theoretical studies were performed on the monocations and monoanions of the iron oxide dimer.[2,8,9,15] For both the monocation $Fe_2O_2^+$ and the monoanion $Fe_2O_2^-$, density functional calculations predicted antiferromagnetic ordering on the two iron centers, while the iron-rich clusters formed high-spin ferromagnetic ground states.[7,8] The bonding scheme of the binuclear dioxides is considerably different from that of bulk oxides or mononuclear oxide clusters as they can form both O–O and metal-metal bonds. The redox and electron-donor properties of the metal oxide dimers can be tuned by coordination of ligands, and among the many possible choices, carbonyl groups deserve consideration, because unsaturated carbonyls are used in the

a)ellie@svr.igic.bas.bg

synthesis of organometallic and transition metal coordination compounds and they remain as building blocks of the structure.[24] Carbon monoxide is a typical σ-donor and forms linear M-CO bonds in the mononuclear carbonyls; π-dative bonding and metal-to-ligand charge transfer (MLCT) is observed mainly with the mid- and end-row elements with filled d-shell and this results in population of the CO vacant π^* antibonding orbitals – typical examples are the hexacarbonyls of Cr and Mo, also the pentacarbonyl of Fe.[25]

In the present study we examine $(FeO)_2$ clusters and their isomers with peroxide bridging bonds by DFT and the ordering by energy of structural isomers in different electronic states is validated by the coupled cluster method. Their relative stability and bonding scheme for different spin multiplicities are elucidated. The bonding of dioxygen to the iron dimer Fe_2 proceeds in dissociative and non-dissociative way. Dioxides $Fe_2(\mu\text{-}O)_2$ are formed by dissociation of molecular dioxygen to oxygen atoms and all possible structures have been considered: ring-shaped and chain-shaped. Clusters with non-equivalent oxygen atoms were found high above the dissociation limit and are not included in the present study. Peroxides exist in two possible configurations, formed by side-on bonding to the iron dimer, $Fe_2(O_2)$, and bridging $Fe(O_2)Fe$. The side-on bonding results in planar configuration, while the bridging oxygen is part of either distorted tetrahedral or chain-like structures. Upon attachment of carbonyl ligands the induced changes in the electron configuration and thermodynamic stability of Fe_2O_2 are assessed. Proton affinities are determined, as well as the electrophilic/nucleophilic properties of the diiron dioxide bare clusters and hexacarbonyls. The reaction path of the water-splitting reaction on hexacarbonyls in singlet and triplet states is traced. Time-dependent DFT calculations are applied to examine electron excitations in the diiron dioxide hexacarbonyls and in their water adsorption complexes.

II. COMPUTATIONAL METHODS

A. Methodology

All calculations were performed with the B3LYP functional, which includes local and non-local terms as implemented in the Gaussian 09 package.[26,27] The standard 6–311+G(d) basis set with diffuse and polarization functions was employed, which consists of the Wachters-Hay all electron basis set for the first transition row, using the scaling factors of Raghavachari and Trucks.[28] In terms of atomic orbitals, the basis set is represented as [10s7p4d1f] for iron, [5s4p1d] for oxygen and carbon. The antiferromagnetic (AFM) coupling of electrons on iron centers was examined for the fixed spin component $S_z = 0$ (singlet), 1 (triplet), 2 (quintet) using the broken-symmetry (BS) approach.[29] The BS approach consists in the localization of the opposite spins on different parts of the molecule to give a mono-determinant representation of the spin exchange interactions within the molecule which reduces the symmetry of the space and spin wavefunctions with respect to that of the nuclear framework. The BS wavefunction is thus not a pure spin state; it is an eigenstate of S_z, but not of $\hat{S}^2$. Coupled-cluster singles and doubles, including non-iterative triples, CCSD(T)[30] single-point calculations have been performed for the bare clusters with the B3LYP-optimized geometries to validate the ordering of isomers in different spin states by energy; for the ordering of the lowest states the Brueckner orbital coupled cluster method BD(T) with additional perturbative estimate of the effects of triple excitations was also applied.[31] The minima on the potential energy surfaces for the allowed spin multiplicities were identified by the absence of negative eigenvalues in the diagonalized Hessian matrix; transition states were characterized by the presence of a single imaginary frequency. The synchronous transit-guided quasi-Newton (STQN) method was used for the transition state optimizations.[32,33] Intrinsic reaction coordinate calculations (IRC) were performed to confirm the structure of the transition states and for evaluating activation energies.[34] The global minimum for the diiron dioxide hexacarbonyl was determined by using different density functionals: B3LYP, B3PW91,[27,35] the Coulomb attenuated modification (CAM) of B3LYP[36] and the non-hybrid functional BPW91[35] (supplementary material).[61] The configuration interaction method with single excitations (CIS)[37] along with time-dependent DFT[38] were used to determine the excitation energies of the ground state carbonylated clusters $Fe_2O_2(CO)_6$ to the low-lying triplet states. The excitation energies in the water adsorption complexes were also calculated; reoptimization of the ground states was performed when different density functionals were applied. Dispersion effects were taken into account in studying water adsorption and splitting by using the empirical formula of Grimme.[39] The dispersion correction according to this formula depends on the number of bonds with intermediate length in the structure, as it has a cutoff for shorter bonds. The formation of water adsorption complexes would thus increase dispersion. The bond populations and charge distributions were examined by natural bond orbital (NBO) analysis.[40] This method yields results that are rather insensitive to basis set enlargement and reveals both covalent and non-covalent effects in molecules. Magnetic moments at the atoms (μ) were calculated as a difference between α and β natural populations. Biorthogonalization did not reveal unmatched orbitals in the ground state configurations. Pearson absolute electronegativity (χ) and hardness (η) were calculated according to the formulas $\chi = (I + A)/2$; $\eta = (I - A)/2$, where I denotes the ionization energy and A is the electron affinity.[41]

B. Method validation

Detailed theoretical studies have been applied to the monoxide FeO and the dioxide FeO_2 in their ground states and low-lying excited states, some of which are closely spaced.[9,10,12,13] The gradient-corrected density functionals without inclusion of Hartree-Fock exchange, such as PW91, BPW91 were preferred in a number of studies[7–9] and for iron-rich oxide clusters Fe_nO, the BPW91 functional was recommended.[7] Though BPW91 provides reliable structures and photodetachment energies, transition metal-oxygen dissociation energies are often overestimated by non-hybrid density functionals, as well as by the meta-GGA TPSS

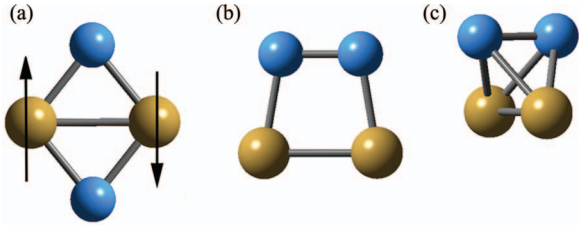

FIG. 1. Dioxides and peroxides with Fe_2O_2 stoichiometry. (a) Fe_2O_2 with planar rhombic structure in the state of the global minimum, (b) planar $Fe_2(O_2)$ with C_{2v} symmetry, and (c) non-planar $Fe(O_2)Fe$, also with C_{2v} symmetry. Iron atoms are brown (larger balls) and oxygen atoms are blue (smaller balls).

functional.[14] The properties of FeO in its ground state $^5\Delta$ are properly described by the B3LYP functional: bond length of 1.614 Å vs 1.616 Å from experiment;[42] the adiabatic electron affinity is 1.476 eV vs the experimental value of 1.49450 ± 0.00022 eV.[43] Fe-Fe bonds are present in most of the di-iron dioxide clusters and in their hexacarbonyls, therefore it is worth evaluating the capability of B3LYP to describe adequately such bonds. The B3LYP calculated bond length of the iron dimer Fe_2 in its $^9\Sigma_g^-$ ground state is 2.112 Å, slightly higher than the experimental one of 2.02 ± 0.02 Å;[44] the calculated dissociation energy is 1.004 eV vs 1.14 ± 0.02 eV from experiment,[45,46] and the electron affinity is 0.874 eV vs the experimental value of 0.902 ± 0.008 eV.[46] Coordination to iron cation centers – of either weakly bound inert gas atoms,[47] or electron-donor ligands,[48–50] were studied using the B3LYP functional and excellent agreement with experimental data was reached. Therefore, B3LYP was selected for geometry optimizations and frequency calculations in the present study and the 6–311+G(d) basis set proved to be large enough to reliably assess both the bare clusters and their hexacarbonyls since optimization of the ground state clusters with the 6–311+G(2df) basis led to bond length changes of less than 0.003 Å and angle changes within 0.02°. As the BS solutions are not pure spin states[51] various methods have been proposed for correcting the energy of the low-spin state among which approximate spin projection was widely applied, particularly for studies of diradicals.[52,53] The spin-unrestricted coupled cluster (CC), and BD methods are less affected by spin contamination than the HF method and are normally employed without projection. Spin projection operators are not recommended for density functional methods as such procedures can lead to significant errors.[52] Such corrections are not used in the present study, because they were found to be very small: less than 2×10^{-3} eV for the bare clusters and less than 10^{-3} eV for the hexacarbonyl complexes.

III. STRUCTURE AND BONDING OF THE CYCLIC IRON OXIDE DIMERS $(FeO)_2$ AND THEIR PEROXIDE ISOMERS $Fe_2(O_2)$

A. Electronic structure and magnetic properties of dioxides and peroxides

All of the optimized bare clusters – dioxides and peroxides – contain a Fe–Fe bond with bond length varying in the range 2.0–2.8 Å. The geometries, corresponding to the ground state isomers are shown in Figure 1.

The planar rhombic diiron dioxide with antiferromagnetically ordered electrons on the iron centers is found as the global minimum in the $2Fe + O_2$ system. The magnetic moment at the iron centers is high, 3.44 μB (Table I), similar to that in the dianion $Co_2O_2^{2-}$.[54] The calculated bond lengths for Fe–Fe (2.275 Å) and Fe–O (1.808 Å) indicate a nearly identical structure with the one obtained by BPW91 calculations.[13] In the high spin state $^9B_{1g}$, the cluster is distorted along the O–O axis and the magnetic moment at oxygen atoms is higher. The planar cyclic dioxide clusters are of the highest stability for all allowed spin multiplicities and large energy gaps separate them from the peroxide configurations, Figure 2. The dioxide in $^7B_{2u}$ state has a nearly identical geometry with the antiferomagnetic (AFM) dioxide. The local magnetic moment on iron atoms is, however, higher in the AFM state, being close to the value for the ferromagnetic $^9B_{1g}$ state. The AFM ordering is thus a key factor in stabilizing the structure of rhombic dioxides. The energy of stabilization of the antiferromagnetic state from the $^7B_{2u}$ state is higher at the B3LYP level (0.69 eV), compared to the BPW91 calculated one (0.12 eV). The planar peroxide with side-on bonded

TABLE I. Bond lengths, bond angles, magnetic moments on atoms (μ, Bohr magnetons) and energies [a] (eV) for dioxides $(FeO)_2$ and for the peroxide-isomers $Fe_2(O_2)$ and $Fe(O_2)Fe$. States, lying higher than 5 eV above the global minimum, are included in the supplemental material.[61]

Cluster/symmetry	State	R_{Fe-O} (Å)	R_{O-O} (Å)	R_{Fe-Fe} (Å)	∠OFeO, ∠FeOO[b](deg)	Dihedral ∠FeFeOO (deg)	μ_{Fe}	μ_O	ΔE_{tot} B3LYP	ΔE_{tot} CCSD(T)
Fe_2O_2, D_{2h}	^{1}**A**	1.808	2.812	2.275	102.1	0.0	3.44	0.00	**0.000**	**0.000**
							−3.44	0.00		
	^{7}**B$_{2u}$**	1.807	2.813	2.276	102.0	0.0	3.00	0.00	**0.688**	**0.886**
	^{9}**B$_{1g}$**	1.868	2.954	2.288	104.5	0.0	3.52	0.48	**1.184**	**1.136**
	^{5}**B$_{1g}$**	1.766	2.580	2.412	93.8	0.0	1.86	0.14	**2.572**	**2.199**
	^{3}**B$_{1g}$**	1.761	2.579	2.398	94.2	0.0	0.85	0.15	**3.311**	**3.207**
$Fe_2(O_2)$, C_{2v}	^{9}**A$_1$**	1.846	1.454	2.536	107.0	0.0	3.81	0.19	**3.709**	**3.943**
	^{7}**A$_2$**	1.827	1.483	2.106	99.8	0.0	2.86	0.14	**4.992**	**5.064**
$Fe(O_2)Fe$, C_{2v}	^{7}**B$_1$**	1.992	1.540	2.422	67.3	71.3	2.83	0.17	**4.612**	**5.073**

[a] ΔE_{tot} – total energy difference relative to the ground state energy of neutral Fe_2O_2: $E_{tot} = -2677.920360$ hartree for B3LYP (zero-point correction included); −2675.33426 hartree for CCSD(T). See Table 1S for Brueckner doubles calculations in the supplementary material.[61]

[b] ∠OFeO for oxide clusters with separated oxygen atoms and for non-planar dioxygen clusters containing bridging O–O bonds; ∠FeOO for planar clusters with bridging or side-on bonded O_2.

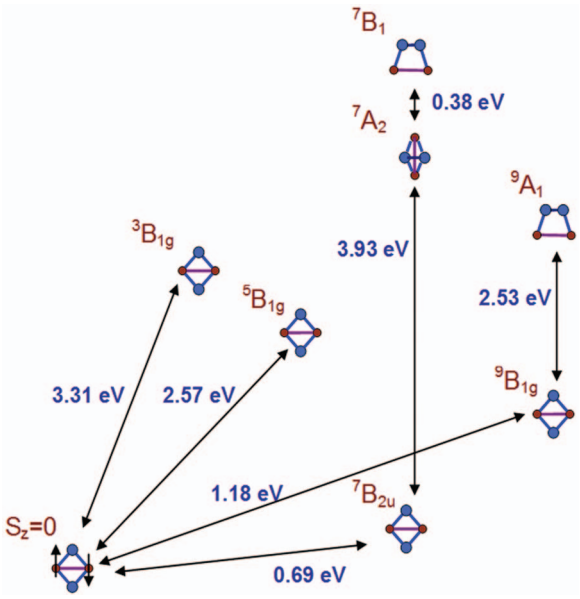

FIG. 2. The ground states corresponding to the different isomeric Fe_2O_2 clusters and local minima lying within 5 eV above the global minimum, grouped according to spin multiplicity. Fe atoms are small brown circles and O atoms are blue. The arrows denote the energy difference ΔE_{tot}, corresponding to adiabatic transitions (Zero-point corrections included).

dioxygen $Fe_2(O_2)$ has a $^9A_1$ ground state with high local magnetic moment at the iron centers and minor magnetization at oxygen. In the septet multiplicity channel, the bridging peroxide configuration $Fe(O_2)Fe$ becomes more stable than the planar one. The Fe–O bonds vary in the range 1.71–1.87 Å in the planar clusters; they are lengthened to 1.90–2.00 Å in the non-planar peroxides. In the ground states of both the planar and non-planar peroxides, the Fe–Fe bonds are elongated by more than 0.15 Å compared to the ground state dioxide; a lengthened Fe–Fe bond is observed also for the ground state $^{10}A_g$ of the dioxide monoanion, Table II. The photoelectron spectrum of the monoanion presented a complicated structure – an adiabatic electron affinity of 2.36 eV was determined and a binding energy of 2.8 eV was deduced; a broad peak of low intensity was observed around 1.5 eV.[3] Our calculations predict a high-spin ground state $^{10}A_g$ of the monoanion with lengthened Fe–Fe bond and a shortened O–O internuclear distance as compared to the neutral clusters in low-lying states. An antiferromagnetic state of the monoanion was also found and it differs in structure from the antiferromagnetic neutral dioxide by a strongly elongated O–O internuclear distance.

The Brueckner orbital coupled cluster method BD(T) and Coupled cluster CCSD(T) energy calculations, based on the B3LYP calculated geometries of the anions in different spin state confirm the ordering of states by energy, though larger energy differences are estimated as compared to the B3LYP calculated values. While the CCSD(T) and BD(T) values reach very good agreement, they coincide with B3LYP only on the ground state of the monoanion. Though the experimental photoelectron spectrum has complicated features, if the CCSD(T) or BD(T) values would be used to calculate the adiabatic electron affinities, bands in the region below 1 eV would be predicted in the spectrum, which were not observed experimentally.[3] The discrepancy between the B3LYP and CCSD(T) or BD(T) energies for the excited states of the monoanion possibly results from applying the B3LYP geometry in these calculations, while a different geometry would be obtained by optimization at the coupled-cluster or Brueckner doubles level of theory. When looking at the B3LYP results, a number of photodetachment processes can be predicted, Table III, with energies varying in the range 1.00–2.60 eV. The ^8A_g to $^9B_{1g}$ transition can be expected to have a significant impact, because of the minimum geometry change required. The vertical detachment energies are close by value to the adiabatic electron affinities for transitions leading to the neutral cluster in $^9B_{1g}$ state.

B. The nature of Fe–Fe bonds and cluster reactivity

The rhombic dioxides bear significant ionic character of the Fe–O bonds, while the peroxides are largely covalent, evidenced by the natural charge distribution, Table IV. Similar orbital population is found for the high-spin dioxides in $^9B_{1g}$ and $^7B_{2u}$ states and the antiferromagnetic state of the dioxide, but the SOMO – LUMO gap is larger for the latter cluster, which is the global minimum. In the antiferromagnetic ground state of the neutral Fe_2O_2 and its monoanion $Fe_2O_2^-$ the planar D_{2h} molecular symmetry is retained, but the α and β orbital representations differ from those in high-spin state as they account for the opposite spin moments at the two iron centers, Table IVS (supplementary material).[61] The clusters in ferromagnetic high-spin states have smaller SOMO – LUMO gaps compared to the clusters in antiferromagnetic state. The molecular orbitals (MO), which contribute to the Fe–Fe bond formation in the dioxide, are highly delocalized, Figure 3. In all planar clusters the angles ∠FeOFe are close to or smaller than 90° and bonds are formed by overlap of the 3d orbitals of the Fe atoms with non-hybrid AOs of oxygen atoms. The $8a_g$ and the $5b_{2u}$ MOs contribute to σ-bond and π-bond formation in the plane of the cluster. The $8a_g$ MO results from the overlap of the $3d_{z^2}$ AOs of Fe and O $2p_y$,$2p_z$ orbitals; the $5b_{2u}$ MO is formed with participation of Fe $3d_{yz}$ AOs and O

TABLE II. Bond lengths, bond angles, magnetic moments on atoms (μ, Bohr magnetons) and energies[a] (eV) for the planar rhombic monoanion $(FeO)_2^-$.

Cluster[b]	State	$R_{Fe\text{-}O}$ (Å)	$R_{O\text{-}O}$ (Å)	$R_{Fe\text{-}Fe}$ (Å)	∠OFeO (deg)	μ_{Fe}	μ_O	ΔE_{tot} B3LYP	ΔE_{tot} CCSD(T)	ΔE_{tot} BD(T)
$(FeO)_2^-$	$^{10}A_g$	1.871	2.711	2.580	92.8	4.08	0.42	**−1.351**	**−1.346**	**−1.358**
	^2A	1.888	3.051	2.225	107.8	3.66	0.09	**−1.002**	**−0.685**	**−0.693**
						−2.83	0.09			
	^8A_g	1.888	3.051	2.225	107.8	3.24	0.26	**−0.866**	**−0.358**	**−0.380**

[a]Energies relative to the neutral cluster ground state.
[b]Notations as in Table I.

TABLE III. Calculated electron affinities (EA, eV) for low-lying states of the dioxide Fe_2O_2 and vertical detachment energies (VD, eV) for the monoanions in the denoted electronic states.[a]

Reaction	EA	Vertical transition	VD
Fe_2O_2, D_{2h}, $^1A + e^- \rightarrow Fe_2O_2^-$, C_{2v}, $^2\mathbf{A}$	1.00	$^2\mathbf{A} \rightarrow {}^1A$	1.21
Fe_2O_2, D_{2h}, $^7B_{2u} + e^- \rightarrow Fe_2O_2^-$, D_{2h}, $^8\mathbf{A_g}$	1.55	$^8\mathbf{A_g} \rightarrow {}^7B_{2u}$	1.80
Fe_2O_2, D_{2h}, $^9B_{1g} + e^- \rightarrow Fe_2O_2^-$, D_{2h}, $^8\mathbf{A_g}$	2.05	$^8\mathbf{A_g} \rightarrow {}^9B_{1g}$	2.10
Fe_2O_2, D_{2h}, $^9B_{1g} + e^- \rightarrow Fe_2O_2^-$, D_{2h}, $^{10}\mathbf{A_g}$	2.54	$^{10}\mathbf{A_g} \rightarrow {}^9B_{1g}$	2.59

[a]Zero-point correction included.

$2p_y$,$2p_z$ AOs. The Fe d_{xz} orbital overlap with O $2p_x$ AOs form the $3b_{3u}$ π-bonding MO, which is delocalized above and below the molecular plane. Another highly delocalized $1b_{1g}$ MO is formed with the participation of the Fe $3d_{x^2-y^2}$ and the O $2p_y$ orbitals.

The partial occupancy of the Fe 4s and 4p AO in the ground state clusters, Table IV, indicate the presence of 3d4s and, in the hexacarbonyls, 3d4s4p hybridization. According to natural orbital population analysis, the Fe 3p AOs in the bare clusters are core orbitals with energies below −2.0 hartree and the Fe 4p AOs have energies in the range 0.05–0.30 hartree, close to the energies of the Fe 4s AOs, 0.10–0.15 hartree. In the hexacarbonyls, both the Fe 4s and the Fe 4p AOs are shifted to higher energy, more significantly the 4s levels (up to 0.75 hartree). The Fe 4p AOs are thus involved to a larger extent in hybridization with the 3d orbitals. The Fe $3d^n$ AOs have typically energies of −0.35 to −0.25 hartree in both the bare clusters and in the hexacarbonyls. A representative example of 3d4s4p hybridization is illustrated in the formation of the $10a_g$ delocalized Fe–Fe and Fe–O bonding MO. The orbitals contributing to the Fe–Fe bond are highly delocalized, with presence of 4s and 4p component. The SOMO in the planar dioxides is a non-bonding orbital with predominantly oxygen lone-pair character, and the LUMO is a typical antibonding MO. In the planar peroxides, the SOMO is an O–O and Fe–Fe bonding MO, while the LUMO is an antibonding orbital as in dioxides, Figure 4. In both the planar and non-planar peroxides, the high occupancy of the Fe 4s orbital indicates that 3d4s hybridization on Fe atoms has major contribution to the formation of Fe-Fe bonds. The frontier orbitals in the non-planar peroxides bear different character: the SOMO is non-bonding MO, with contribution of O and Fe lone-pair AOs, but the LUMO is a delocalized Fe–Fe and O–O bonding orbital, with main component at the Fe atoms and the Fe–Fe bond.

Both the dioxide and the peroxide in their ground states are stable towards fragmentation with release of molecular oxygen, see Table V, and their stability is considerably higher compared to the mononuclear iron oxide and peroxide.[14] The preferred dissociation path is towards the monomer, FeO. The dioxides in either antiferromagnetic or high-spin states require more than 200 kJ mol^{-1} for dissociation to FeO, while the ground state planar peroxide is weakly endothermic and the non-planar peroxides are of even lower thermodynamic stability. The iron oxide dimers can participate in both nucleophilic reactions (via the oxygen centers) and electrophilic reactions (via the iron centers). The proton affinity of Fe_2O_2 is higher compared to that of molecular oxygen (421.0 kJ mol^{-1}) or hydroxyl groups (593.2 kJ mol^{-1}),[55] but smaller than the calculated value for $(CoO)_2$, 827 kJ mol^{-1}.[54] Water molecules are adsorbed at the iron centers and the Fe–O_w internuclear distances within 2.097–2.103 Å were calculated for one and two adsorbed molecules. The Fe–OH_2 interactions are predominantly electrostatic, as the calculated natural partial charges on water molecule oxygen atoms are within −0.90; −0.92 *e*, close to the value for unbound water molecule (−0.92 *e)* and slightly smaller than the natural charges of the bridging oxygen atoms within the rhombic cluster, see Table IV. The calculated adsorption energies are 94.9 kJ mol^{-1} for the first adsorbed water molecule and 84.8

TABLE IV. HOMO(SOMO) – LUMO gaps (eV), natural population analysis[a] and natural charges (q_M, *e*) for $(FeO)_2$ and $Fe_2O_2(CO)_6$ clusters in diamagnetic, antiferromagnetic (AFM), and in ferromagnetic (FM) high-spin states.

Cluster	HOMO(SOMO) – LUMO	q_{Fe}	q_O	Fe 3d	Fe 4s	Fe 4p
$Fe_2O_2(CO)_6$; $^1\mathbf{A'}$	3.26	− 0.80	− 0.53	7.36	0.38	1.05
AFM states						
Fe_2O_2	3.30	1.08	− 1.08	6.48	0.25	0.19
$Fe_2O_2(CO)_6$; ^3A	2.92	− 0.76	− 0.55	7.33	0.38	1.03
		− 0.41		7.03		
$Fe_2(O_2)(CO)_6$; ^1A	3.88	− 0.69	− 0.25	7.33	0.39	0.96
FM, high-spin states						
Fe_2O_2; $^7B_{2u}$	2.81	0.97	− 0.97	6.56	0.29	0.17
Fe_2O_2; $^9B_{1g}$	2.19	1.08	− 1.08	6.49	0.22	0.21
$Fe_2(O_2)$; $^9A_1$	2.27	0.56	− 0.56	6.44	0.81	0.19
$Fe(O_2)Fe$; $^7B_1$	2.06	0.62	− 0.62	6.71	0.47	0.18
$Fe_2O_2(CO)_6$; $^5A'$	2.87	− 0.46	− 0.55	7.07	0.37	1.00

[a]The α and β natural populations of Fe_2O_2 clusters are listed in Table IVS in the supplementary material.[61]

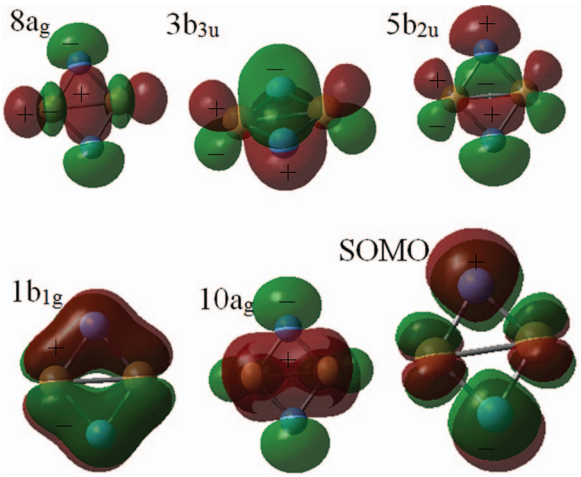

FIG. 3. The delocalized symmetrical frontier orbitals of Fe_2O_2 in ferromagnetic state $^7B_{2u}$: the $2b_{1g}$ SOMO and orbitals with contribution to the Fe–Fe bond for a standard orientation of the rhombic planar cluster in the σ_{yz} plane and with the Fe atoms lying along the z-axis. Positive phases of MOs are marked with + (red) and negative with – (green). Orbital energies, hartree: $8a_g$ (−0.3953), $3b_{3u}$ (−0.3882), $5b_{2u}$ (−0.3861), $1b_{1g}$ (−0.3822), $10a_g$ (−0.2621), $2b_{1g}$ SOMO (−0.2370). In the anti-ferromagnetic state, the corresponding $\alpha + \beta$ orbitals have similar shape.

kJ mol^{-1} for the second one. No magnetic interactions occur between the adsorbed molecules and the dioxide cluster, and the antiferromagnetic ordering at the iron centers is retained. The bending vibration of the water molecule is slightly blueshifted upon adsorption – from 1605 to 1630 cm^{-1}, while the antisymmetric stretching vibration is redshifted by 20 cm^{-1}.

The adsorption of water in this case is non-dissociative, as the water molecules interact only with the Fe centers of Fe_2O_2 and their orientation is not favorable for the formation of hydrogen bonds with the oxygen atoms. Recent DFT studies of water splitting on hematite[19] and on metal surfaces[56] revealed the importance of hydrogen bonds formed either with a surface oxygen atom (hematite) or within the water dimers,

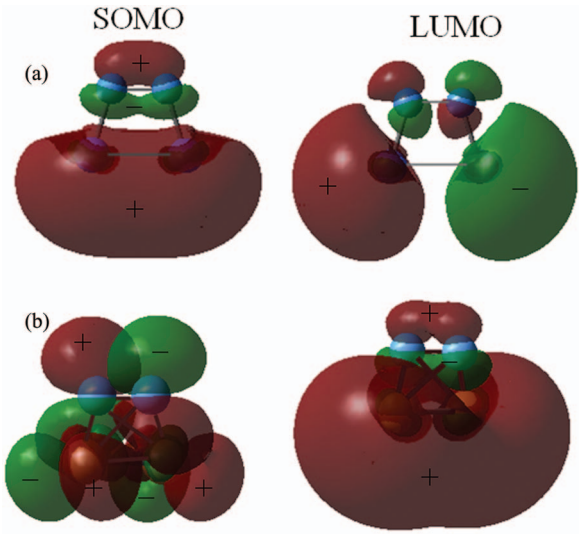

FIG. 4. The SOMO and LUMO orbitals in (a) planar and (b) non-planar peroxides. Legend as in Figure 3.

TABLE V. Calculated dissociation energies (D_{zpe}, kJ mol^{-1}) [a], proton affinities (PA, kJ mol^{-1}) [a], absolute electronegativities (χ, eV), and hardness (η, eV) of the ground state dioxides Fe_2O_2, $Fe_2O_2(CO)_6$ and peroxides $Fe_2(O_2)$, $Fe_2(O_2)(CO)_6$.

	D_{zpe}	PA	χ	η
$(FeO)_2 \rightarrow 2FeO$	335	730	4.43	4.00
$Fe_2(O_2) \rightarrow 2FeO$	−22.6		4.57	2.58
$(FeO)_2 \rightarrow 2Fe + O_2$	665			
$Fe_2(O_2) \rightarrow 2Fe + O_2$	307			
$Fe_2O_2(CO)_6 \rightarrow Fe_2(CO)_6 + O_2$	414	974	4.88	2.95
$Fe_2(O_2)(CO)_6 \rightarrow Fe_2(CO)_6 + O_2$	315	808	4.90	4.17
$Fe_2O_2(CO)_6 \rightarrow 2FeO + 6CO$	686			
$Fe_2(O_2)(CO)_6 \rightarrow 2FeO + 6CO$	587			
$Fe_2O_2(CO)_6 \rightarrow 2FeO(CO)_3$	280			
$Fe_2O_2(CO)_6 \rightarrow (CO)_3FeO_2Fe(CO)_2 + CO$	93			
$Fe_2O_2(CO)_6 \rightarrow (CO)_2FeO_2Fe(CO)_2 + CO$	129			
$Fe_2O_2(CO)_6 \rightarrow (CO)_3FeO_2Fe(CO) + CO$	146			

[a]Zero-point correction included.

adsorbed on transition metal surfaces. Our attempts to find a reaction path for water splitting on the bare clusters were not successful: no other stationary points could be detected up to 4.7 eV above the energy of the adsorption complex $Fe_2O_2(H_2O)$. For the diiron dioxide the proton affinity is relatively low and the absolute electonegativity and hardness have similar values, Table V. This explains the lack of activity in water splitting and it cannot be expected that the bare dioxides would be active in redox reactions either.

IV. STRUCTURE AND BONDING OF CARBONYLATED DIOXIDE $(FeO)_2$ AND PEROXIDE $Fe_2(O_2)$

A. Electronic and magnetic structure of low-spin and high-spin states

In the hexacarbonyls of Fe_2O_2 and $Fe_2(O_2)$ the properties of the iron-oxygen core are altered in terms of structure, stability, magnetic ordering and electron distribution. The planar Fe_2O_2 configuration is no longer favored and a nearly planar Fe_2O_2 ring is retained only in the $^5A'$ state. The dioxides $Fe_2O_2(CO)_6$ have butterfly-like orientation of the carbonyl groups, while in the peroxide $Fe_2(O_2)(CO)_6$ they are rotated around the Fe–Fe axis, Figure 5. Compared to the bare clusters, the Fe–Fe internuclear distances in hexacarbonyls are lengthened (>2.6 Å) and the peroxide does not contain

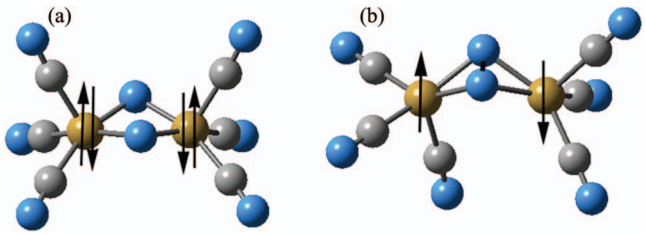

FIG. 5. Ground state isomeric hexacarbonyls of the Fe_2O_2 clusters. (a) The global minimum, diamagnetic $Fe_2O_2(CO)_6$. (b) Antiferromagnetic singlet ground state of the peroxide, $Fe_2(O_2)(CO)_6$. Iron atoms are brown (light grey, with arrows denoting the α and β spin magnetic moments), oxygen atoms are blue (dark grey), and carbon atoms are grey.

TABLE VI. Bond lengths, bond angles, magnetic moments on atoms (μ, Bohr magnetons) and energies [a] (eV) for $Fe_2O_2(CO)_6$ and $Fe_2(O_2)(CO)_6$ complexes, calculated by B3LYP.

Cluster model	State	$R_{Fe\text{-}O}$ (Å)	$R_{O\text{-}O}$ (Å)	$R_{Fe\text{-}Fe}$ (Å)	$R_{Fe\text{-}C}$ (Å)	∠FeOFe (deg)	Dihedral ∠OFeOFe (deg)	μ_{Fe}	μ_O	ΔE_{tot}, B3LYP
$Fe_2O_2(CO)_6$	$^1A'$	1.833	2.415	2.648	1.77–1.86	92.5	23.8	0.00	0.00	**0.000**
	^3A	1.841	2.419	2.730	1.77–2.06	95.8	13.4	1.77	0.26	**0.223**
		1.824						−0.17		
	$^5A'$	1.838	2.590	2.614	1.83–1.90	91.0	2.2	1.72	0.40	**0.444**
$Fe_2(O_2)(CO)_6$	^1A	1.950	1.450	3.108	1.82–1.91	105.7	58.0	1.10	0.00	**0.870**
								−1.10		

[a] ΔE_{tot} – total energy difference relative to the ground state energy of neutral $Fe_2O_2(CO)_6$ with $E_{tot} = -3358.117976$ hartree; zero-point correction included.

a Fe–Fe bond, while the O–O distances are shortened. The local magnetic moments on iron centers are smaller in the carbonylated clusters and they do not exceed 2 μB, Table VI. The carbonylated dioxide $Fe_2O_2(CO)_6$ in diamagnetic ground state $^1A'$ is the most stable structure. It has a non-planar Fe_2O_2 core, but the deviation from planarity is smaller than in the ground state of the peroxide, $Fe_2(O_2)(CO)_6$. A significant negative net charge is introduced in the Fe_2O_2 core upon carbonylation, Table IV, and the electron-donor capacity of the iron oxide hexacarbonyls is much higher than in their Co analogs.[54] The strong interaction with the carbonyl groups is evidenced by the relatively short Fe–C bond lengths. The carbonyl groups in $Fe_2O_2(CO)_6$ are not equivalent and the two carbonyl groups which point above the oxygen atoms of the Fe_2O_2 ring and lie in a plane intersecting the ring along the Fe–Fe axis, form stronger Fe–C bonds of length 1.77 Å. The C–O bond lengths are, however, negligibly changed. The calculated CO stretching vibration undergoes a relatively small shift to lower frequencies (2185 cm^{-1}) compared to the free CO molecule (2212 cm^{-1}), which indicates a minor contribution of π-electron back-donation from the metal to the vacant π^* antibonding orbitals of CO. The SOMO – LUMO gaps increase upon CO coordination – most significantly for the peroxide, which becomes thermodynamically more stable as hexacarbonyl, Table V. Unlike the bare cluster peroxide, antiferromagnetic coupling is favored in its hexacarbonyl complex. In all Fe_2O_2 hexacarbonyls, the population of the Fe AOs is strongly increased compared to the bare dioxides and peroxides. The net occupancy of the Fe 4p orbital corresponds to an extra electron; the population of the 4s orbital is also increased, but less significantly, and the 3d orbitals population exceeds 7 electrons, Table IV. The electronic states of the hexacarbonyls are more closely spaced, in contrast to the bare clusters, and the peroxide lies by 0.87 eV above the global minimum, compared to 3.7 eV in the bare clusters.

The release of molecular oxygen becomes more favorable for the hexacarbonyls, compared to the bare clusters, as the binding of the carbonyl groups to Fe is strong, Table V. The loss of one carbonyl group requires 93 kJ mol^{-1}; for the loss of a second one from the other Fe center, the energy increases to 129 kJ mol^{-1}, whereas the dissociation of a second carbonyl group from the same Fe atom is less favorable. The monomer, FeO, forms a stable tricarbonyl compound and therefore, the decomposition of the diiron dioxide hexacarbonyls to two iron oxide tricarbonyl molecules is more favorable than the release of molecular oxygen. This reaction is less endothermic than the dissociation of the bare cluster dimer to iron monoxide. Examination of the reaction path of decomposition with elongation of two Fe–O bonds on opposite sides of the rhombic core in the bare cluster and in the hexacarbonyl reveals, however, that lengthening of the bonds by 0.45 Å requires 158 kJ mol^{-1} for the bare cluster vs 198 kJ mol^{-1} for the hexacarbonyl, which indicates a higher barrier to the hexacarbonyl decomposition reaction. The smaller hardness value for the dioxide $Fe_2O_2(CO)_6$ is an indicator for the ease of reaching singlet-to-triplet state excitations and for the increased nucleophilic character of the Fe_2O_2 ring.

It is worth noting that for the peroxide hexacarbonyl both electronegativity and hardness increase, while for the ground state dioxide hexacarbonyl the absolute hardness is smaller than for the bare cluster. This is related to the value of the HOMO – LUMO gap, which in the singlet ground state of the hexacarbonyl is slightly smaller than the SOMO – LUMO gap of the bare dioxide and much smaller than that of the peroxide hexacarbonyl. The antiferromagnetic coupling contributes to the higher stability of the diiron dioxide bare cluster in the state of the global minimum and of the diiron peroxide hexacarbonyl. The proton affinity of the hexacarbonyls is much higher, compared to the bare clusters and compares with the calculated proton affinity of $Co_2O_2(CO)_6$, 1033.6 kJ mol^{-1}.[54]

The Fe–O bonds are largely covalent in the hexacarbonyls unlike the bare dioxides Fe_2O_2, which bear typically ionic character. The strong effect of electron transfer from the carbonyl groups to the metal atoms induces a negative charge to the Fe_2O_2 core and the iron centers bear a larger negative partial charge than the oxygen centers, Table IV. The orbitals which contribute to the Fe–Fe bond in the carbonylated dioxide are delocalized over Fe and O atoms and also participate in binding to the CO groups, Figure 6. They have their analogs in the bare clusters. The 35a′ MO is delocalized over the Fe_2O_2 ring and results from the overlap of the $3d_{z^2}$ AOs of Fe and O $2p_y$ orbitals; the 36a′ MO contributes to Fe–O, Fe–Fe and Fe–C bond formation and its main components are the Fe $3d_{xz}$ AOs and O $2p_x$ AOs. The Fe d_{yz} orbital overlap with O $2p_y$ AOs form the 37a′ Fe–O π-bonding MO. The 39a′ orbital contributes to the Fe–Fe bond, the Fe–O bonds and the delocalized Fe–C π-bonds; it results from 3d4s4p hybridization at the Fe centers and overlap of the resulting hybrid orbitals with the O 2p AOs and the C 2p AOs. The nature of

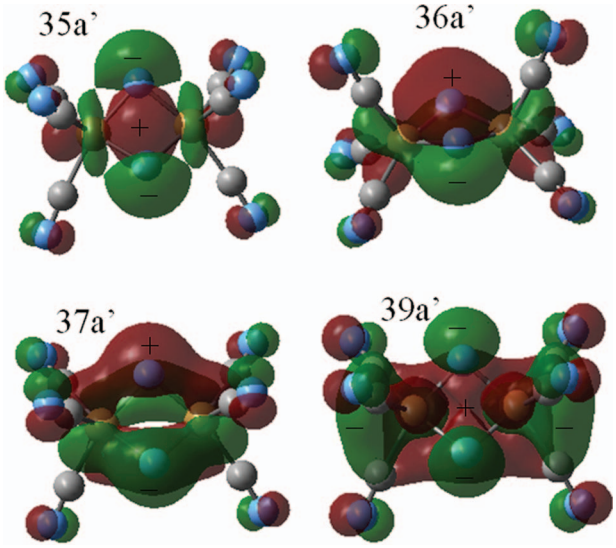

FIG. 6. The delocalized bonding orbitals of $Fe_2O_2(CO)_6$ which contribute to the Fe–Fe bond. Positive phases of MOs are marked with + (red) and negative with – (green). Orbital energies, hartree: 35 a′ (−0.4020), 36 a′ (−0.3685), 37 a′ (−0.3594), 39 a′ (−0.2761).

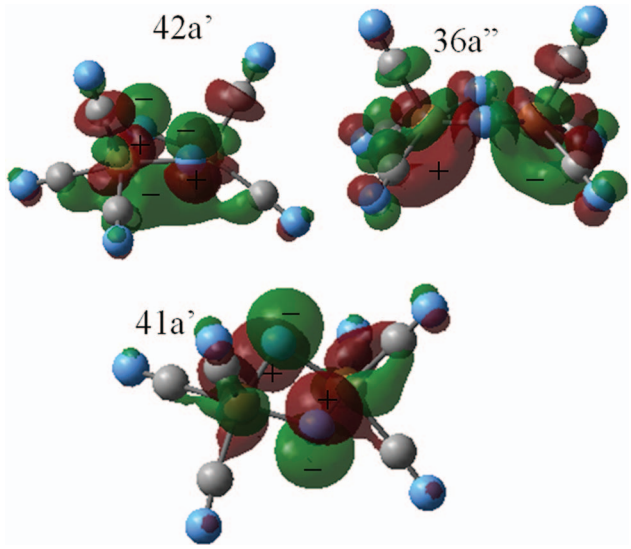

FIG. 7. The frontier orbitals in $Fe_2O_2(CO)_6$ with orbital energies, hartree: 41 a′ HOMO (−0.2359), 42 a′ LUMO (−0.1161), and 36 a″ LUMO + 1 (−0.1149). Legend as in Figure 6.

the HOMO(SOMO) and LUMO orbitals is markedly different from that in bare dioxides and peroxides, Figure 7. The HOMO consists of an oxygen lone pair, similarly to the planar dioxide, but a bonding Fe-CO component emerges in the hexacarbonyl. The LUMO is also constituted by an oxygen lone-pair and a broad delocalized Fe–Fe bonding component. The next to the LUMO orbital, LUMO + 1, is a typically antibonding one.

B. Vibrational frequencies

The irreducible representation for the normal vibrations in planar dioxides reads as $\Gamma[Fe_2O_2, D_{2h}] = 2a_g(R) + b_{3g}(R) + b_{1u}(IR) + b_{2u}(IR) + b_{3u}(IR)$ for $(FeO)_2$ positioned in the σ_{yz} plane and Fe atoms lying along the z-axis. The IR-active vibrations originate from the antisymmetric Fe–O stretching (b_{1u}), the Fe–O–Fe bending (b_{2u}) modes, and the out-of-plane b_{3u} mode. In all IR-active modes oxygen atoms shift in the same direction, thus providing a strong change in dipole moment. For the dioxide Fe_2O_2, the experimental IR frequencies in solid N_2 and Ar are nearly identical, the frequency of the bending b_{1u} mode being shifted by less than 20 cm^{-1} in solid N_2. The two bands of high intensity in the spectrum, at 657–661 cm^{-1}, and 517–536 cm^{-1}, which correspond to the b_{2u} and b_{1u} modes, are in good agreement with the B3LYP calculated frequencies, Table VII.

The normal modes of the planar peroxides with side-on bonded dioxygen $Fe_2(O_2)$ and the non-planar peroxides with bridging dioxygen span very similar irreducible representations: $\Gamma[Fe_2(O_2), C_{2v}] = 3a_1(IR,R) + 2b_2(IR,R) + a_2(R)$ and $\Gamma[Fe(O_2)Fe, C_{2v}] = 3a_1(IR,R) + b_1(IR,R) + b_2(IR,R) + a_2(R)$. The highest frequency vibration in the peroxide-clusters corresponds to the O–O stretching mode and it is found in the range of 740–860 cm^{-1} for the ground state peroxides. The O–O vibration of the non-planar cluster $Fe(O_2)Fe$ appears in the lower-energy part of this range (744 cm^{-1}); however, in the carbonylated cluster $Fe_2(O_2)(CO)_6$ this mode

TABLE VII. Vibrational frequencies and zero-point energies of the ground state diiron dioxide clusters. [a]

State	Fe_2O_2 $^1\mathbf{A}$	Fe_2O_2 exp.	$Fe_2(O_2)$ $^9\mathbf{A_1}$	$Fe(O_2)Fe$ $^7\mathbf{B_2}$
ω (cm^{-1})	719 a_g	670 ± 70 [b]	853 a_1	744 a_1
	690 b_{2u}	660.6 [c]	575 a_1	442 b_1
	528 b_{1u}	657.3 [d]	525 b_2	418 a_1
	440 b_{3g}		217 a_1	189 a_1
	302 a_g	517.4 [e]	100 b_2	179 b_2
	187 b_{3u}	535.5 [d]	64 a_2	174 a_2
ZPE (kJ mol^{-1})	17.1		14.0	12.8

[a]Vibrations with dominant participation of the Fe_2O_2 ring in carbonylated clusters are presented in Table VIIS in the supplementary material.[61]
[b]Gas-phase estimated value from laser photoelectron spectroscopy, Ref. 3.
[c]IR spectra in solid Ar, Refs. 4, 5, and 22.
[d]IR spectra in solid N_2, Ref. 6.
[e]IR spectra in solid Ar, Refs. 1, 4, and 5.

is shifted to 888 cm^{-1}. Peroxides have not been detected so far by IR spectroscopy, as the bare clusters appear as endothermic according to our study, but they become stable as hexacarbonyls and it can be expected that anchoring to surfaces is another way to increase their stability.

C. Reactivity of the Fe_2O_2 hexacarbonyls. Water adsorption and dissociation

The presence of a stable low-lying triplet state of $Fe_2O_2(CO)_6$ allows singlet-to-triplet excitations from the state of the global minimum, $^1A'$. The singlet-triplet transitions are forbidden, thus they have a low probability, but longer lifetime, which certainly depends on the energy of the transition and the possibility to reach a stable triplet state. The antiferromagnetic triplet state of $Fe_2O_2(CO)_6$ lies by only 0.22 eV above the ground state and the geometries of the singlet and triplet states differ as to the Fe–Fe, Fe–CO bond lengths and the degree of deviation from planarity, Table VI. Time-dependent (TD) calculations with the B3LYP functional yield excitation energy of 0.37 eV, which corresponds to 3388 nm, or the mid-wavelength IR region. The second singlet-triplet excitation energy of 1.04 eV corresponds to 1194 nm or the NIR region. The calculated lowest singlet-singlet excitation energy is 1.58 eV, thus it is higher than the transitions to the two low-lying triplet states. The accuracy of a TD-DFT calculation is largely governed by the choice of exchange-correlation functional, and particularly on the amount of exact exchange included. Time-dependent Hartree-Fock theory (TDHF, 100% exact exchange) significantly underestimates triplet excitation energies in cases when a triplet instability problem in the ground state wave function is present and it was considered that this error could be overcome using configuration interaction singles (CIS).[38,39,57,58] Calculations of the Hartree-Fock stability for dinuclear transition metal complexes with antiferromagnetic interactions is a difficult task because of convergence problems, therefore we applied the strategy of using density functionals with different amount of exact exchange. B3LYP includes 20% of exact exchange, which does not depend on the interelectron distance r_{12}. The Coulomb-attenuated functionals, where the amount of exact exchange increases with r_{12} have been shown to yield improved long-range, Rydberg and charge-transfer excitation energies, at the same time providing good quality for local excitations.[59,60] The Coulomb-attenuated modification of B3LYP, CAM-B3LYP, includes 19% of exact exchange, which increases with r_{12} to 65%.[36] Best agreement between the calculated excitation energies is obtained using B3LYP and B3PW91, though the latter functional yields higher energy for the second excitation, $^1A' \rightarrow {}^3A''$, Table VIII. CAM-B3LYP and BPW91 yield similar energies for both excitations, but the first transition, $^1A' \rightarrow {}^3A'$, is underestimated, compared to the hybrid functional calculations with B3LYP and B3PW91.

The CIS results agree with hybrid functionals on the lowest transition, but significantly underestimate the second one. Doubles correction to the CIS calculated $^1A' \rightarrow {}^3A''$ energy yield 1.33 eV, which exceeds the upper limit marked by B3PW91; however, the first transition, $^1A' \rightarrow {}^3A'$, is severely overestimated. The electron transition from the HOMO (41 a′) to the LUMO (42 a′) orbital in $Fe_2O_2(CO)_6$ bears ligand to metal charge transfer character (LMCT) as the HOMO consists of oxygen lone pairs and a Fe–C bonding component to the two carbonyl groups, which lie in a plane perpendicular to the Fe_2O_2 ring, bisecting it along the Fe–Fe axis, Figure 7. The LUMO retains the oxygen lone-pair features and has a significant Fe–Fe bonding component. The transition to the LUMO + 1 orbital (36 a″) would weaken the bonds in the Fe_2O_2 core.

TABLE VIII. Vertical excitation energies (eV) of the ground state cluster $Fe_2O_2(CO)_6$ to the low-lying triplet states.

	Transition	
Method/functional TDDFT	$^1A' \rightarrow {}^3A'$	$^1A' \rightarrow {}^3A''$
B3LYP	0.37	1.04
B3PW91	0.40	1.18
CAM-B3LYP	0.17	0.90
BPW91	0.16	0.91
CIS	0.39	0.49
CIS(D)	1.11	1.33

Water adsorption by the hexacarbonyl complexes is less exothermic compared to the bare clusters. On the peroxide complex, no adsorption occurs. The adsorption energy for the singlet ground state of the dioxide is 39.1 kJ mol^{-1}, slightly smaller than the triplet state, 42.4 kJ mol^{-1}. The singlet state reaction path is the more favorable one for water splitting, as the energy barrier is very small, 0.2 kJ mol^{-1}, so dissociation is spontaneous, exothermic, with calculated change of the Gibbs free energy of 112 kJ mol^{-1}, Figure 8. The water molecule forms weak hydrogen bonds with both oxygen atoms of the Fe_2O_2 core, with $H–O_{core}$ bond lengths of 2.070 Å for singlet state and 2.114 Å for triplet state, nearly equal to the $Fe–O_w$ bond lengths, 2.085 Å and 2.110 Å, for the singlet and triplet adsorption complex respectively, Figure 9(a). The O–H bonds in the adsorbed water molecule are slightly lengthened to 0.976 Å in the triplet and to 0.978 Å in the singlet state complex, compared to the free water molecule, 0.962 Å. The dihedral angle FeOFeO decreases to 5.4° in the singlet state, compared to the ground state of the hexacarbonyl complex, and slightly increases to 13.7° in the triplet state adsorption complex. One could expect an equally small activation energy barrier for the triplet state reaction path, based on the similar water-Fe_2O_2 interaction in the adsorption complex. In the transition triplet state structural rearrangement occurs, with the oxygen atoms from the Fe_2O_2 core being shifted above the ring plane to provide favorable site for hydrogen bond formation so the dihedral angle reaches 20.2°, Figure 9(b). This results in an activation barrier of 14.1 kJ mol^{-1}, which allows water splitting at room temperature, though the triplet transition state (TS) lies by 32.3 kJ mol^{-1} (0.33 eV) above the singlet TS. On the triplet potential energy surface, the reaction of water splitting is less exothermic, with change in the Gibbs free energy of 48.2 kJ mol^{-1}. The energy separation between singlet and triplet state

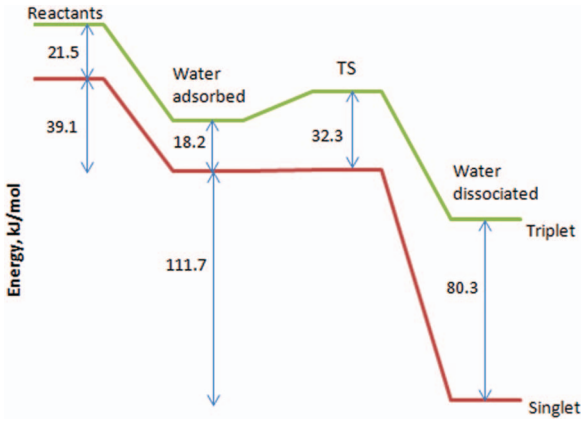

FIG. 8. The reaction path for water splitting along the singlet and triplet potential energy surfaces. Energy barriers are determined at the B3LYP level from IRC path following. Structures are shown in Figure 9.

TABLE IX. Vertical excitation energies (eV) of the ground state singlet adsorption complex $Fe_2O_2(CO)_6(H_2O)$ and the dissociation product $Fe_2O(OH)_2(CO)_6$ to the low-lying triplet and singlet states, calculated with TD DFT.

	$Fe_2O_2(CO)_6(H_2O)$		$Fe_2O(OH)_2(CO)_6$	
Functional	**Singlet → triplet**	**Singlet → singlet**	**Singlet → triplet**	**Singlet → singlet**
B3LYP	0.67	1.63	1.77	2.50
	1.07	1.98	2.02	2.54
	1.61	2.30	2.03	2.75
	0.75	1.73	1.86	2.62
B3PW91	1.16	2.07	2.11	2.66
	1.69	2.41	2.15	2.87
	0.59	1.67	1.87	2.70
CAM-B3LYP	0.90	1.94	1.99	2.78
	1.51	2.31	2.06	2.83

is small for the water adsorption complexes in pre-dissociated state, 18.2 kJ mol^{-1} (0.19 eV) but it increases along the reaction path, reaching 80.3 kJ mol^{-1} (0.83 eV) for the oxy-dihydroxyl complexes, Figure 8.

In the dissociated state, the hydroxyl groups remain coordinated to both iron centers, Figure 9(c). The O–H bond lengths are equal to those in a free water molecule, 0.962–0.963 Å. The nucleophilic properties of the $Fe_2O(OH)_2(CO)_6$ complexes are increased relative to the parent complexes $Fe_2O_2(CO)_6$. The negative natural charges at oxygen atoms are in the range −0.71 to −0.61 *e*, as compared to −0.55, −0.53 *e* in the prior-to-reaction state, Table IV.

The small energy barrier for water splitting appoints the hexacarbonyl complexes of diiron dioxide as perspective candidates for photo- and electrocatalytic conversion of water into fuel ($H_2 + O_2$). For the water adsorption complexes in pre-dissociated and in dissociated state, the time dependent calculations with the B3LYP, B3PW91 and CAM-B3LYP density functionals predict a shift towards higher vertical excitation energies than those of the hexacarbonyl $Fe_2O_2(CO)_6$, Table IX. While for the pre-dissociated state the shift of the lowest singlet-triplet is small, 0.3–0.4 eV, in the dissociated state, the oxy-dihydroxide, all of the six lowest excitation energies are shifted by 0.5–1.0 eV.

The dominant contribution to both the singlet-triplet and singlet-singlet excitations of the pre-dissociated complex belongs to electron excitation from oxygen lone pairs of the Fe_2O_2 core to either of the iron centers – the iron atom without water adsorbed, and the one forming the adsorption site. In the oxy-dihydroxyl complex the electron excitations from the lone-pair orbitals of the bridging oxygen atom to the hydroxyl groups have a major impact. Though shifted to higher energies, the lowest singlet-triplet and singlet-singlet excitations remain in the IR and visible region, thus the activation of both the water adsorption complex and dissociated product, the oxy-dihydroxyl hexacarbonyl of iron, can be achieved by visible light.

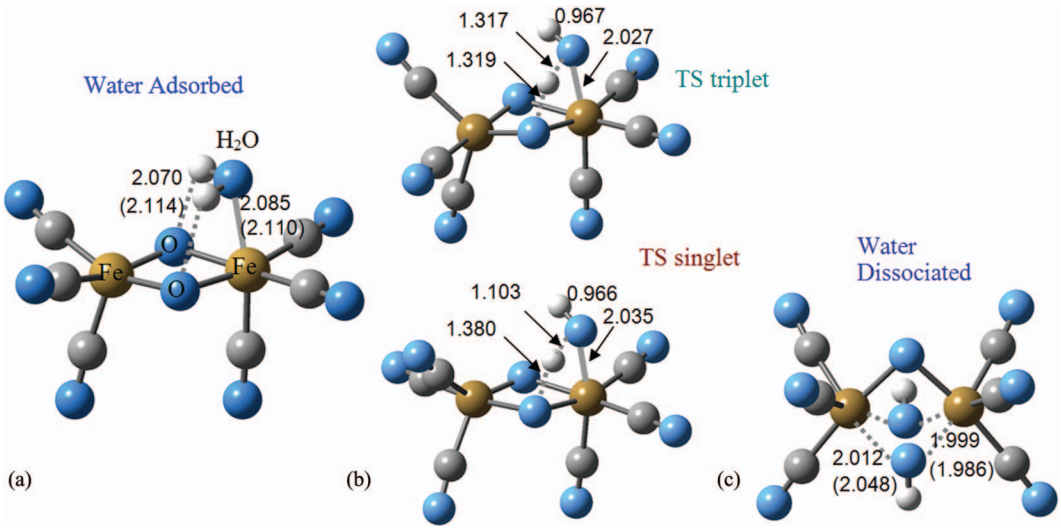

FIG. 9. Structure of the (a) water adsorption complex, (b) transition state, and (c) dissociation product for the reaction path on a singlet and triplet PES. Bond lengths for the triplet state of the adsorption complex and the dissociated product are given in brackets. Legend as in Figure 5.

V. CONCLUSIONS

The DFT studies of clusters with Fe_2O_2 stoichiometry indicate that the dioxides with planar rhombic structure are the dominant species among the bare clusters. In the state of the global minimum antiferromagnetic ordering is observed at iron centers. The local minima configurations of peroxides with side-on bonded and bridging dioxygen have been revealed. Large energy gaps separate the peroxides from the dioxides (>2.5 eV), but they become smaller in the hexacarbonyls (<0.9 eV). All of the bare clusters contain Fe–Fe bonds and this is valid also for the diiron dioxide hexacarbonyls; only in the hexacarbonyl of the peroxide with bridging dioxygen the iron centers are separated by large internuclear distance of 3.108 Å. The ground state of the peroxide configuration is $^9A_1$ and corresponds to a planar four-member ring. The next low-lying state, $^7B_1$, which keeps an O–O bond, is non-planar with dioxygen oriented perpendicular to the Fe-Fe bond. The dioxide has pronounced ionic features, while the peroxides are predominantly covalent. The binding energy of water adsorbed at the bare dioxide clusters (87.0 kJ mol^{-1}), is larger than that in the hexacarbonyl complexes (39.1–42.4 kJ mol^{-1}), but dissociation of water on the bare clusters does not occur. Carbonylation introduces significant changes in the Fe_2O_2 core: HOMO(SOMO) – LUMO gaps are increased, the energy differences between low-lying states are reduced, proton affinity is increased, as well as the absolute electronegativity. The singlet-to-triplet state energy gaps are much smaller in the carbonylated clusters and electron excitations require low-energy activation. Water splitting on the singlet potential energy surface (PES) proceeds spontaneously; for the triplet PES a small energy barrier of 14.1 kJ mol^{-1} was calculated. In the transition state hydrogen bonds between an adsorbed water molecule and an oxygen atom from the Fe_2O_2 core of the hexacarbonyl complexes are formed. The hydroxyl groups in the product of dissociation remain coordinated to both iron atoms. The calculated vertical excitation energies in the pre-dissociated state (water adsorption complex) and in the dissociation product (oxydihydroxyl complex) indicate that activation can be achieved by visible light. The present study demonstrates how the properties of the active site (Fe_2O_2) are modified by the coordination of carbonyl ligands. The hexcarbonyl complexes of diiron dioxide are promising materials for photo- or electro-catalytic water-to-fuel conversion.

ACKNOWLEDGMENTS

The computational results have been achieved in part using the Vienna Scientific Cluster (VSC-1). E.L.U. acknowledges CPU time at the high-performance BG08-MADARA computer cluster of the Bulgarian Academy of Sciences.

[1]S. Chang, G. Blyholder, and J. Fernandez, Inorg. Chem. **20**, 2813 (1981).
[2]D. Schroeder, A. Fiedler, J. Schwarz, and H. Schwarz, Inorg. Chem. **33**, 5094 (1994).
[3]H. Wu, R. Desai, and L.-S. Wang, J. Am. Chem. Soc. **118**, 5296 (1996); **118**, 7434 (1996).
[4]L. Andrews, G. V. Chertihin, A. Ricca, and C. W. Bauschlicher, Jr., J. Am. Chem. Soc. **118**, 467 (1996).
[5]G. V. Chertihin, W. Saffel, J. T. Yustein, L. Andrews, M. Neurock, A. Ricca, and C. W. Bauschlicher, Jr., J. Phys. Chem. **100**, 5261 (1996).
[6]L. Andrews, G. V. Chertihin, A. Citra, and M. Neurock, J. Phys. Chem. **100**, 11235 (1996).
[7]G. L. Gutsev, Ch. W. Bauschlicher, Jr, H.-J. Zhai, and L.-S. Wang, J. Chem. Phys. **119**, 11135 (2003).
[8]N. M. Reilly, J. Ulises Reveles, G. E. Johnson, J. M. del Campo, S. N. Khanna, A. M. Ko1ster, and A. W. Castleman, Jr., J. Phys. Chem. C **111**, 19086 (2007); N. M. Reilly, J. Ulises Reveles, G. E. Johnson, S. N. Khanna, and A. W. Castleman, Jr., J. Phys. Chem. A **111**, 4158 (2007).
[9]G. L. Gutsev, S. N. Khanna, B. K. Rao, and P. Jena, J. Phys. Chem. A **103**, 5812 (1999); G. L. Gutsev, B. K. Rao, and P. Jena, *ibid.* **104**, 11961 (2000); **104**, 5374 (2000).
[10]F. Grein, Int. J. Quantum Chem. **109**, 549 (2009)
[11]C. N. Sakellaris, E. Miliordos, and A. Mavridis, J. Chem. Phys. **134**, 234308 (2011).
[12]M. F. A. Hendrickx and K. R. Anam, J. Phys. Chem. A **113**, 8746 (2009); M. F. A. Hendrickx and V. T. Tran, J. Chem. Theory Comput. **8**, 3089 (2012); V. T. Tran and M. F. A. Hendrickx, *ibid.* **7**, 310 (2011)
[13]G. L. Gutsev, C. A. Weatherford, P. Jena, E. Johnson, and B. R. Ramachandran, Chem. Phys. Lett. **556**, 211 (2013); D. R. Roy, R. Robles, and S. N. Khanna, J. Chem. Phys. **132**, 194305 (2010).
[14]E. L. Uzunova, J. Phys. Chem. A **115**, 1320 (2011); **115**, 10665 (2011); E. L. Uzunova, H. Mikosch, and G. St. Nikolov, J. Chem. Phys. **128**, 094307 (2008); E. L. Uzunova, G. St. Nikolov, and H. Mikosch, ChemPhysChem **5**, 192 (2004).
[15]K. S. Molek, C. Anfuso-Cleary, and M. A. Duncan, J. Phys. Chem. A **112**, 9238 (2008).
[16]G. A. Somorjai, *Introduction to Surface Chemistry and Catalysis* (J. Wiley & Sons, NY, 1994).
[17]Y. Lin, G. Yuan, S. Sheehan, S. Zhou, and D. Wang, Energy Environ. Sci. **4**, 4862 (2011).
[18]I. Cesar, A. Kay, J. A. Gonzalez Martinez, and M. Grätzel, J. Am. Chem. Soc. **128**, 4582 (2006).
[19]M.-T. Nguyen, N. Seriani, and R. Gebauer, J. Chem. Phys. **138**, 194709 (2013).
[20]X. Liu, S. K. Ibrahim, C. Tard, and C. Pickett, J. Coord. Chem. Rev. **249**, 1641 (2005).
[21]Y. Gong, M. Zhou, and L. Andrews, Chem. Rev. **109**, 6765 (2009).
[22]G. V. Chertihin, A. Citra, L. Andrews, and C. W. Bauschlicher, Jr., J. Phys. Chem. A **101**, 8793 (1997).
[23]Z. Cao, M. Duran, and M. Solà, J. Chem. Soc., Faraday Trans. **94**, 2877 (1998).
[24]H. Ogino, S. Inomata, and H. Tobita, Chem. Rev. **98**, 2093 (1998).
[25]H. B. Gray and C. J. Ballhausen, J. Am. Chem. Soc. **85**, 260 (1963); T. P. Goumans, A. W. Ehlers, M. C. van Hemert, A. Rosa, E. J. Baerends, and K. Lammertsma, *ibid.* **125**, 3558 (2003).
[26]M. J. Frisch, G. W. Trucks, H. B. Schlegel *et al.*, Gaussian 09, Revision D.01, Gaussian, Inc., Wallingford, CT, 2009.
[27]A. D. Becke, J. Chem. Phys. **104**, 1040 (1996); **98**, 5648 (1993); C. Lee, W. Yang, and R. G. Parr, Phys. Rev. B **37**, 785 (1988); B. Miehlich, A. Savin, H. Stoll, and H. Preuss, Chem. Phys. Lett. **157**, 200 (1989).
[28]A. J. H. Wachters, J. Chem. Phys. **52**, 1033 (1970); P. J. Hay, *ibid.* **66**, 4377 (1977); K. Raghavachari and G. W. Trucks, *ibid.* **91**, 1062 (1989); P. J. Hay and W. R. Wadt, *ibid.* **82**, 270 (1985).
[29]T. Lovella, F. Himo, W.-G. Han, and L. Noodleman, Coord. Chem. Rev. **238–239**, 211 (2003); R. A. Torres, T. Lovell, L. Noodleman, and D. A. Case, J. Am. Chem. Soc. **125**, 1923 (2003); L. Noodleman, J. Chem. Phys. **74**, 5737 (1981).
[30]J. Cizek, Adv. Chem. Phys. **14**, 35 (1969); G. D. Purvis and R. J. Bartlett, J. Chem. Phys. **76**, 1910 (1982); J. A. Pople, R. Krishnan, H. B. Schlegel, and J. S. Binkley, Int. J. Quantum Chem. **14**, 545 (1978).
[31]N. C. Handy, J. A. Pople, M. Head-Gordon, K. Raghavachari, and G. W. Trucks, Chem. Phys. Lett. **164**, 185 (1989); R. Kobayashi, N. C. Handy, R. D. Amos, G. W. Trucks, M. J. Frisch, and J. A. Pople, J. Chem. Phys. **95**, 6723 (1991).
[32]T. A. Halgren and W. N. Lipscomb, Chem. Phys. Lett. **49**, 225 (1977).
[33]C. Peng, P. Y. Ayala, H. B. Schlegel, and M. J. Frisch, J. Comput. Chem. **17**, 49 (1996).
[34]J. P. Perdew, J. A. Chevary, S. H. Vosko, K. A. Jackson, M. R. Pederson, D. J. Singh, and C. Fiolhais, Phys. Rev. B **46**, 6671 (1992); **48**, 4978 (1993).
[35]K. Fukui, Acc. Chem. Res. **14**, 363 (1981); H. P. Hratchian and H. B. Schlegel, J. Chem. Phys. **120**, 9918 (2004).
[36]T. Yanai, D. Tew, and N. Handy, Chem. Phys. Lett. **393**, 51 (2004).

[37]J. B. Foresman, M. Head-Gordon, J. A. Pople, and M. J. Frisch, J. Phys. Chem. **96**, 135 (1992).
[38]R. Bauernschmitt and R. Ahlrichs, J. Chem. Phys. **104**, 9047 (1996); Chem. Phys. Lett. **256**, 454 (1996); F. Furche and R. Ahlrichs, J. Chem. Phys. **117**, 7433 (2002).
[39]S. Grimme, J. Antony, S. Ehrlich, and H. Krieg, J. Chem. Phys. **132**, 154104 (2010).
[40]A. E. Reed, L. A. Curtiss, and F. Weinhold, Chem. Rev. **88**, 899 (1988); F. Weinhold and J. E. Carpenter, *The Structure of Small Molecules and Ions* (Plenum, 1988).
[41]R. G. Pearson, Inorg. Chem. **27**, 734 (1988).
[42]A. J. Merer, Annu. Rev. Phys. Chem. **40**, 407 (1989).
[43]G. Drechsler, U. Boesl, C. Bäßmann, and E. W. Schlag, J. Chem. Phys. **107**, 2284 (1997).
[44]H. Purdum, P. A. Montano, G. K. Shenoy, and T. Morrison, Phys. Rev. B **25**, 4412 (1982).
[45]L. Lian, C. X. Su, and P. B. Armentrout, J. Chem. Phys. **97**, 4072 (1992).
[46]D. G. Leopold and W. C. Lineberger, J. Chem. Phys. **85**, 51 (1986); D. G. Leopold, J. Almlöf, W. C. Lineberger, and R. Taylor, *ibid.* **88**, 3780 (1988).
[47]R. Garza-Galindo, M. Castro, and M. A. Duncan, J. Phys. Chem. A **116**, 1906 (2012).
[48]F. Rondinelli, N. Russo, and M. Toscano, Inorg. Chem. **46**, 7489 (2007).
[49]A. Altun and W. Thiel, J. Phys. Chem. B **109**, 1268 (2005); R.-Z. Liao and W. Thiel, *ibid.* **116**, 9396 (2012).
[50]J. M. Mouesca, J. L. Chen, L. Noodleman, D. Bashford, and D. A. Case, J. Am. Chem. Soc. **116**, 11898 (1994).
[51]L. Bertini, M. Bruschi, L. de Gioia, P. Fantuchi, C. Greco, and G. Zampella, Top. Curr. Chem. **268**, 1 (2007).
[52]J. M. Wittbrodt and H. B. Schlegel, J. Chem. Phys. **105**, 6574 (1996); J. Wang, A. D. Becke, and V. H. Smith, Jr., *ibid.* **102**, 3477 (1995); H. B. Schlegel, *ibid.* **92**, 3075 (1988); J. L. Sonnenberg, H. P. Hratchian, and H. B. Schlegel, "Spin Contamination in Inorganic Chemistry Calculations" in *Encyclopedia of Inorganic Chemistry*, 3rd ed. (John Wiley & Sons, Ltd., New York, 2009).
[53]K. Yamaguchi, F. Jensen, A. Dorigo, and K. N. Houk, Chem. Phys. Lett. **149**, 537 (1988); Y. Kitagawa, T. Saito, M. Ito, M. Shoji, K. Koizumi, S. Yamanaka, T. Kawakami, M. Okumura, and K. Yamaguchi, *ibid.* **442**, 445 (2007).
[54]E. L. Uzunova and H. Mikosch, J. Phys. Chem. A **116**, 3295 (2012).
[55]E. P. Hunter and S. G. Lias, J. Phys. Chem. Ref. Data **27**, 413 (1998).
[56]C. Michel, F. Göltl, and Ph. Sautet, Phys. Chem. Chem. Phys. **14**, 15286 (2012).
[57]R. Seeger and J. A. Pople, J. Chem. Phys. **66**, 3045 (1977).
[58]A. Dreuw and M. Head-Gordon, Chem. Rev. **105**, 4009 (2005).
[59]Y. Tawada, T. Tsuneda, S. Yanagisawa, T. Yanai, and K. Hirao, J. Chem. Phys. **120**, 8425 (2004).
[60]G. Cui and W. Yang, Mol. Phys. **108**, 2745 (2010).
[61]See supplementary material at http://dx.doi.org/10.1063/1.4858462 for a full list of calculated electronic states for the Fe_2O_2 clusters and their isomers. Relative energies, calculated by B3LYP and single point coupled cluster calculations using CCSD(T) and BD(T) are presented as Table IS and the alpha-beta natural populations in Table IVS. Optimized geometries of the diiron dioxide hexacarbonyl using different density functional are included in Table VIS. IR frequencies for Fe_2O_2 and their hexacarbonyls are summarized in Table VIIIS.